Minimally disruptive optical control of protein tyrosine phosphatase 1B

Akarawin Hongdusit[a], Peter H. Zwart[b], Banumathi Sankaran[b], and Jerome M. Fox[a*]

[a]Department of Chemical and Biological Engineering, University of Colorado Boulder, 3415 Colorado Avenue, Boulder, CO, 80303
[b]Molecular Biophysics and Integrated Bioimaging, Lawrence Berkeley National Laboratory, Berkeley, CA, 94720

*To whom correspondence should be addressed. E-mail: jerome.fox@colorado.edu

ABSTRACT

Protein tyrosine phosphatases regulate a myriad of essential subcellular signaling events, yet they remain difficult to study in their native biophysical context. Here we develop a minimally disruptive optical approach to toggle the activity of protein tyrosine phosphatase 1B (PTP1B)—an important regulator of receptor tyrosine kinases and a therapeutic target for the treatment of diabetes, obesity, and cancer—and we use that approach to probe both the structure and intracellular function of this enzyme. Our conservative architecture for photocontrol, which consists of a protein-based light switch fused to an allosteric regulatory element, preserves the native structure, activity, and subcellular localization of PTP1B, affords changes in activity that match those elicited by post-translational modifications inside the cell, and permits experimental analyses of the molecular basis of optical modulation. This work provides a framework for using optogenetic systems to examine both the biophysical basis and spatial context of cell signaling.

The enzymatic phosphorylation of tyrosine residues is centrally important to cellular function. It controls the location and timing of cellular differentiation, movement, proliferation, and death[1–4]; its misregulation can cause cancer, diabetes, and neurodegenerative diseases, among other disorders[5–7]. Methods to toggle the activity of phosphorylation-regulating enzymes without interfering with their native structure or cellular organization could, thus, enable detailed analyses of the mechanisms by which cells process essential chemical signals[8,9].

Optogenetic actuators—genetically encoded proteins that undergo light-induced changes in conformation—provide a powerful means of controlling enzyme activity over time and space. As protein fusion partners, they have enabled optical manipulation of biomolecular transport, binding, and catalysis with millisecond and submicron resolution[10,11]. Common strategies to integrate optogenetic actuators into enzymes include (i) attachment near an active site, where they control substrate access[12,13], (ii) insertion within a catalytic domain, where they afford activity-modulating structural distortions[14], and (iii) fusion to N- or C-termini, where they direct subcellular localization[15] or guide domain assembly[16]. These approaches have generated powerful tools for stimulating phosphorylation-mediated signaling networks; their reliance on disruptive structural modifications, however, has precluded their use in both (i) biophysical analyses of native intra-domain control systems (allosteric networks) and (ii) biochemical studies of native regulatory effects—that is, changes in activity that match, rather than artificially exceed, those caused by post-translational modifications of an enzyme under study.

Protein tyrosine phosphatase 1B (PTP1B) is an important regulatory enzyme for which minimally disruptive architectures for photocontrol could prove particularly informative. This enzyme catalyzes the hydrolytic dephosphorylation of tyrosine residues on numerous important proteins; it helps regulate insulin, leptin, and epidermal growth factor signaling and participates

in a diverse set of spatiotemporally complex signaling processes[17]. PTP1B has two intriguing biophysical traits that could be amenable to optogenetic study: (i) Its catalytically essential WPD loop undergoes cyclic, open-and-close motions that control the rate of phosphotyrosine hydrolysis at the active site[18], and its C-terminal α7 helix modulates these motions through an allosteric network that extends over 25 Å across the protein (Fig. 1a). An architecture for photocontrol that makes use of this network could facilitate an analysis of its essential components and, perhaps, reveal its functional role in other PTPs. (ii) PTP1B undergoes several post-translational modifications outside of its active site that cause modest, yet physiologically influential shifts in its activity (i.e., 1.7- 3.1 fold[19,20]; Supplementary Table 1). An optogenetic construct that affords similar changes in activity could serve as an important experimental tool for determining if these changes—rather than the specific post-translational modifications that cause them—give rise to ensuing biochemical effects. Additionally, we note that PTP1B belongs to a class of regulatory enzymes (protein tyrosine phosphatases, or PTPs) that presently lack established optogenetic control systems of any kind.

In this study, we used a protein-based light switch to place the native allosteric regulatory system of PTP1B under optical control. This conservative optogenetic design preserved the native structure and subcellular localization of PTP1B, permitted changes in activity that match those caused by post-translational modifications inside the cell and, when paired with a FRET-based biosensor, enabled spatiotemporal control and measurement of intracellular PTP1B activity. The optogenetic tools developed in this study complement existing methods for studying protein tyrosine kinases (PTKs), which have numerous light-sensitive analogues and FRET-based biosensors[21,22], and demonstrate a new approach for using minimally disruptive control systems to probe both the structure and intracellular function of regulatory enzymes.

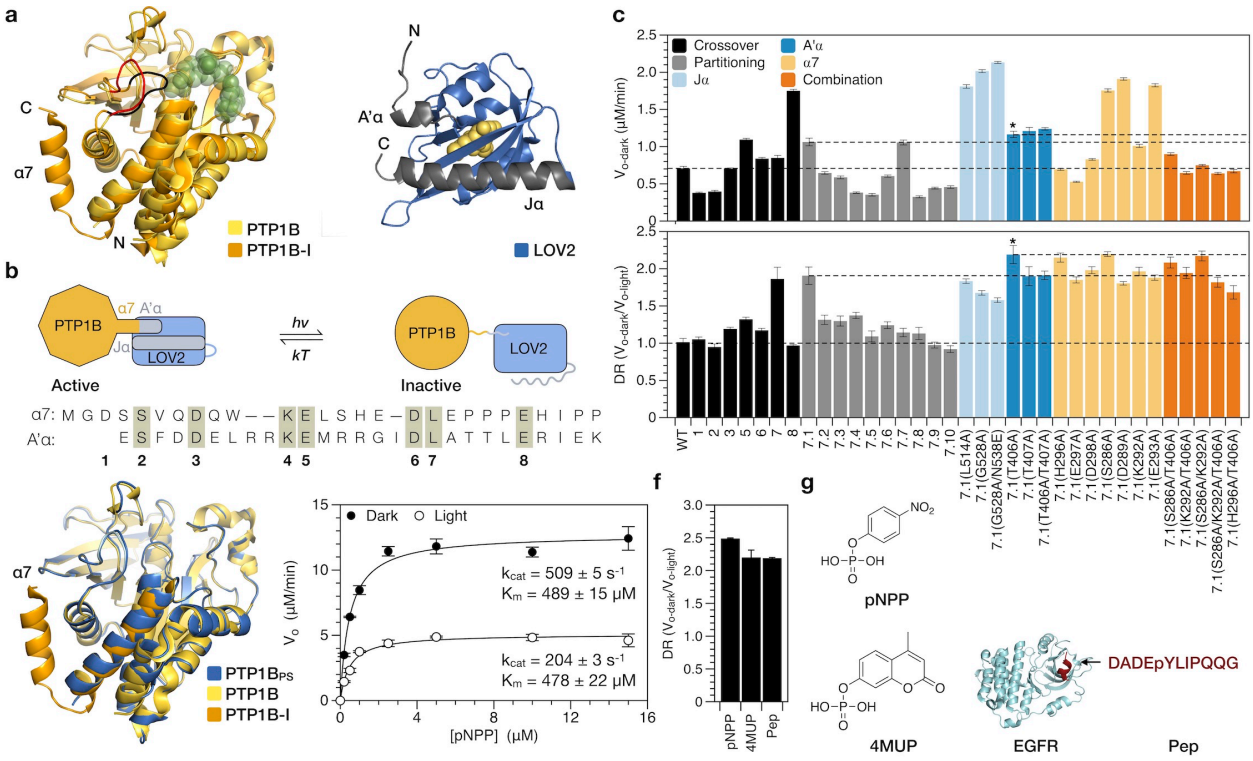

Figure 1 | Minimally disruptive photocontrol of PTP1B. a, Left: An alignment of a competitively inhibited structure of PTP1B (orange, pdb entry 2f71) and an apo structure of PTP1B (yellow, pdb entry 3a5j) highlight an allosteric control system. Closure of the WPD loop (black) over an inhibitor orders the α7 helix; opening of the loop (red) prevents this ordering. Right: A crystal structure of LOV2 (blue pdb entry 2v0w) highlights two terminal α-helices that are stable in the dark state, but not the light state. **b**, Design of a photoswitchable chimera. Light-induced unwinding of the A'α helix of LOV2 destabilizes the α7 helix of PTP1B, causing an allosteric conformational change that inhibits catalysis. We attached the C-terminal α7 helix of PTP1B to the N-terminal A'α helix of LOV2 at homologous crossover points (1-8). **c**, Assays on 4-methylumbelliferyl phosphate (4MUP) show the results of chimera optimization. Construct 7 has the largest dynamic range (DR) of the crossover variants; 7.1 has a higher activity than 7, and 7.1(A406A), termed PTP1B$_{PS}$, has a larger DR than 7.1. **d,** Aligned catalytic domains of PTP1B in three structures: photoswitchable (6ntp), apo (3a5j), and competitively inhibited (2f71,

α6 and α7 only). **e**, An analysis of the activity of $PTP1B_{PS}$ on p-nitrophenyl-phosphate (pNPP) indicates that light affects k_{cat}, but not K_m ($k_{cat\text{-}dark}/k_{cat\text{-}light}$ = 2.50 +/- 0.04). **f**, The DR of $PTP1B_{PS}$ is similar for substrates of different sizes. **g**, Structures of pNPP, 4MUP, and a peptide (PEP) derived from epidermal growth factor receptor (EGFR). Error bars in **c**, **e**, and **f** denote standard error (SE) with $n \geq 6$ independent reactions. Exact sample sizes appear in Supplementary Tables 3 and 4.

RESULTS

Allosteric Photocontrol of PTP1B. We sought to place PTP1B under optical control by using LOV2, the light-sensitive domain from phototropin 1 of *Avena sativa*, to toggle the conformation of its α7 helix. LOV2 derives its optical activity from a noncovalently bound flavin mononucleotide (FMN), which when exposed to blue light, forms an intermolecular carbon-sulfur bond that destabilizes the N- and C-terminal helices of the protein (Fig. 1a)[23]. We hypothesized that attachment of the N-terminal A'α helix of LOV2 to the C-terminal α7 helix of PTP1B would couple (i) light-induced unwinding of the A'α helix to (ii) destabilization of the α7 helix and disruption of WPD loop motions (an established effect of α7 unwinding[24]; Fig. 1b). To our satisfaction, several PTP1B-LOV2 chimeras—each generated by fusing the A'α and α7 helices at a different crossover point—exhibited light-dependent catalytic activity on 4-methylumbelliferyl phosphate (4MUP; Fig. 1c). Fusion of the Jα helix of LOV2 to the N-terminus of PTP1B, by contrast, did not confer photosensitivity (Supplementary Figs. 1a-1b), a result consistent with the large distance between its N-terminus and active site (Fig. 1a).

To enhance the dynamic range (DR = $V_{o\text{-}dark}$ / $V_{o\text{-}light}$) of our most light-sensitive chimera (i.e., construct 7, where DR = 1.8), we used two approaches: First, we attempted to improve communication between the LOV2 and PTP1B domains by reducing the length of the linker between them; similar changes have improved photoswitching in other light-sensitive fusions[25]. Unfortunately, shorter linkers tended to reduce DR. We chose one construct with an unaltered DR—chimera 7.1—for further optimization. Next, we attempted to increase the stability of the dark state over the light state by adding stabilizing mutations to flexible helices. In previous studies of LOV2-based constructs, stabilizing mutations in the Jα helix have improved DR[26,27]. (For Jα and A'α helices, we used established mutations[23,26]; for α7, we replaced solvent-exposed

residues with alanine, which has a high helix propensity[28]). Interestingly, for our chimeras, mutations in the Jα helix improved activity, but reduced photosensitivity, while several mutations in the A'α and α7 helices increased DR (Fig. 1c); overall, the effects of amino acid substitutions in these two helices were non-additive and reached a maximum DR of 2.2 on 4MUP. We chose a single high-DR chimera—7.1(T406A), termed $PTP1B_{PS}$—for further study.

We assessed the structural integrity of the PTP1B domain within $PTP1B_{PS}$ by using X-ray crystallography to examine its dark-state conformation. Intriguingly, although crystals of $PTP1B_{PS}$ were yellow and turned clear when exposed to blue light—a behavior indicative of the presence of LOV2[12,29]—diffraction data permitted placement and refinement of only PTP1B (Supplementary Fig. 2). Detection of LOV2 was likely impeded by two interrelated crystallographic features: (i) a disordered α7 helix, which is unresolvable in apo structures of PTP1B[24], and (ii) variability in the orientation of LOV2 within the crystal lattice (SI Note 1). Fortunately, despite structural disorder, an alignment of the catalytic domains of $PTP1B_{PS}$ and wild-type PTP1B yielded a root-mean-square deviation of 0.30 Å (Fig. 1d). Crystallographic results, thus, suggest that LOV2 does not alter the native conformation of PTP1B.

We explored the mechanism of photomodulation by using kinetic assays to examine the influence of LOV2 on PTP1B-mediated catalysis. In brief, we measured the activity of $PTP1B_{PS}$ on p-nitrophenyl-phosphate (pNPP) in the presence and absence of blue light (455 nm), and we used the initial rates to construct dark- and light-state Michaelis-Menten curves (Fig. 1e). Kinetic data indicate that blue light reduces k_{cat} by 2.5-fold but leaves K_m unaltered. Data collected under repeated illumination, in turn, shows that changes in k_{cat} are reversible (Supplementary Fig. 3c). The isolated influence of LOV2 on k_{cat} is consistent with an allosteric mechanism in which it modulates catalytically essential loop motions.

To assess the maximum DR achievable with our control system, we removed the α7 helix of PTP1B; that is, we used an α7-less variant as a model for a maximally photoswitched form of this enzyme. Helix removal lowered k_{cat} by 2.9-fold, suggesting that $PTP1B_{PS}$ has a DR that is 85% of the maximum achievable value for a photoswitch that inhibits catalytic activity by unwinding the α7-helix (Supplementary Fig. 3a). Importantly, this DR is within the range of DRs of previously developed light-sensitive signaling enzymes used to elicit physiologically relevant cellular responses to optical stimuli (DRs ~1.7-10[12,30]; Supplementary Table 17) and matches physiologically influential changes in activity caused by post-translational modifications of PTP1B that occur outside of its active site (i.e., phosphorylation, proteolysis, and sumoylation, which reduce/enhance PTP1B activity by 1.7- 3.1 fold[19,20]; Supplementary Table 1).

A control system that allosterically modulates catalytically essential loop motions should—in contrast with a control system that competitively inhibits the active site—exhibit a modulatory effect that is independent of substrate size (and binding affinity). To test the substrate dependence of $PTP1B_{PS}$, we measured its DR on pNPP, 4MUP, and a phosphorylated peptide (Fig. 1f). The DRs for these substrates differed by less than 15% (Fig. 1g); this similarity suggests that the magnitude of photocontrol in our system is, in fact, substrate independent.

Biophysical Analysis of Photocontrol. We designed our chimeras to exploit conformational changes in the N-terminal A'α helix of LOV2; the results of crystallographic and spectroscopic analyses of this photoswitch, however, indicate that its N- and C- terminal helices work together to transduce conformational changes across the protein[23,31]. To examine the contribution of these helices to the photoresponse of one of our most light-sensitive chimeras (7.1), we modified them with disruptive mutations (i.e., we added charged residues at buried

sites[31,32]). For both helices, disruptive mutations reduced light-dependent catalytic activity as effectively as C450M, a "dark state" mutation that prevents the formation of the cysteine adduct in LOV2; complete removal of the Jα helix had the same effect (Fig. 2a). Our results thus indicate that both A'α and Jα helices are necessary to control catalytic activity.

An NMR analysis of PTP1B dynamics has shown that mutations in its L11 loop can disrupt allosteric communication between its α7 helix and WPD loop[24]. To confirm the contribution of allostery to photocontrol, we modified chimera 7.1 with a mutation known to exert such an effect: Y152A/Y153A. This modification reduced DR by ~25%, a disruption distinct from the conservative/beneficial effects of alanine substitutions in the α7 helix (Fig. 2a). The sensitivity of DR to mutations in the L11 loop indicates that the native allosteric network of PTP1B is, indeed, necessary for LOV2-based modulation of catalytic activity.

We hypothesized that our most photoswitchable chimeras might exhibit large changes in secondary structure between light and dark states—changes that result primarily from disordering of the A'α, Jα, and α7 helices from highly ordered conformations. To test this hypothesis, we used circular dichroism (CD) spectroscopy to compare optically induced shifts in α-helical content ($\delta_{222} = [CD_{222\text{-dark}}-CD_{222\text{-light}}]/CD_{222\text{-dark}}$; Fig. 2b). Intriguingly, changes were large for the chimeras with light-dependent catalytic activities but spanned a range of values for low-DR constructs, (Fig. 2c). The one-way dependence of DR on δ_{222} indicates that changes in α-helical conformation are necessary, but not sufficient for photocontrol.

We speculated that chimeras with large changes in α-helical content (i.e., δ_{222}) but light-insensitive catalytic activities (i.e., low DRs) might suffer from weak conformational coupling between the LOV2 and PTP1B domains. To study this coupling, we carried out two experiments. In the first, we examined the thermal recovery of LOV2 from the light state by illuminating

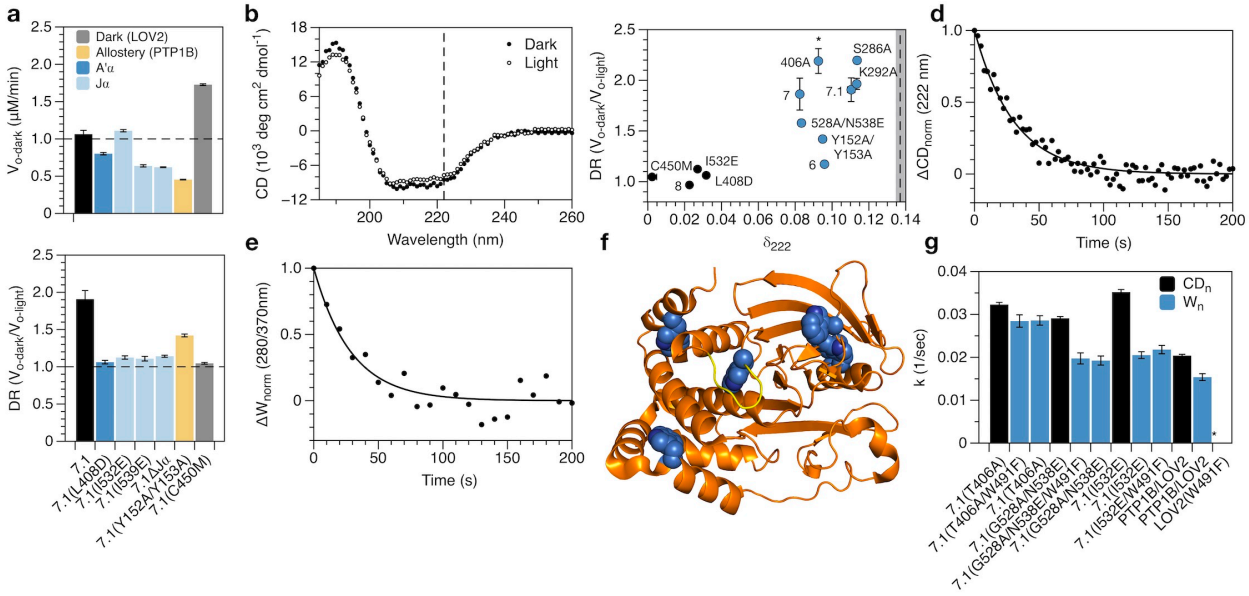

Figure 2 | Analysis of allosteric communication in PTP1B$_{PS}$. a, Mutations that prevent adduct formation in LOV2 (C450M), destabilize the A'α and Jα helices (I532E, I539E, and ΔJα), or disrupt the allosteric network of PTP1B (Y152A/Y153A) reduce the photosensitivity of 7.1 and, with the exception of I532E and C450M, lower its specific activity. **b**, Exposure of PTP1B$_{PS}$ to 455 nm light reduces its α-helical content (i.e., the mean residue ellipticity [MRE] at 222 nm). **c**, An analysis of different chimeras indicates that light-induced changes in α-helical content (i.e., $\delta_{222} = [CD_{222\text{-dark}}\text{-}CD_{222\text{-light}}]/CD_{222\text{-dark}}$, or the fractional change in MRE at 222 nm) are necessary, but not sufficient for light-sensitive catalytic activity (i.e., high DR). Mutations correspond to variants of 7.1; chimeras with large values of δ_{222} appear in blue; and the dashed line indicates δ_{222} for equimolar amounts of free PTP1B and LOV2. **d-e**, Thermal recovery of (**d**) α-helical content (i.e., the change in MRE at 222 nm normalized by the full change over 250 seconds) and (**e**) tryptophan fluorescence (i.e., the change in fluorescence normalized by the full change over 250 seconds) of PTP1B$_{PS}$. **f**, A crystal structure of PTP1B (pdb entry 2f71) shows the locations of six tryptophan residues (blue) and the WPD loop (yellow). **g**, Kinetic constants for thermal recovery are larger for α-helical content than for tryptophan fluorescence (the latter

of which is not affected by W491). This discrepancy is smallest for PTP1B$_{PS}$ (i.e., 7.1(T406A)). Error bars in **a**, **c**, and **g** denote SE with $n \geq 6$ independent reactions. Exact sample sizes appear in Supplementary Tables 6 and 7.

PTP1B-LOV2 chimeras with blue light and, subsequently, measuring the return of α-helical content in the dark (Fig. 2d). A link between the conformation of LOV2 and α-helical content is supported by (i) the sensitivity of δ_{222} to disruptive mutations in LOV2 and (ii) the insensitivity of δ_{222} to the catalytic response of PTP1B (i.e., activity-modulating structural changes in PTP1B, which differ between high- and low-DR chimeras, do not affect δ_{222}). In the second experiment, we examined the thermal recovery of PTP1B by measuring the return of tryptophan fluorescence in the dark (Fig. 2e). A link between the conformation of PTP1B and tryptophan fluorescence is supported by (i) the existence of six tryptophan residues in PTP1B (Fig. 2f) and (ii) the insensitivity of recovery kinetics to the removal of W491, the only tryptophan in LOV2 (Fig. 2g). Intriguingly, kinetic constants for thermal recovery were higher for α-helical content than for tryptophan fluorescence, an indication that LOV2 reverts to its dark state more quickly than PTP1B. This discrepancy was (i) smallest for $PTP1B_{PS}$, the highest-DR construct, (ii) moderate for 7.1(G528A/N538E), a construct with an intermediary DR, and (iii) largest for 7.1(I532E), a Jα-destabilized mutant without light-dependent catalytic activity (Fig. 2g). This pattern in recovery kinetics provides direct evidence that strong inter-domain conformational coupling is necessary for photocontrol of PTP1B activity.

Optogenetic Analysis of Allosteric Regulation in PTPs. Recent studies suggest that allosteric regulation is a conserved attribute of PTPs[24,33]; the shared regulatory function of the α7 helix (or its PTP-specific equivalent), however, remains unclear. To examine the generality of α7-based allostery, we attached the LOV2 domain of $PTP1B_{PS}$ to the C-terminal helix of T-cell protein tyrosine phosphatase (TCPTP). This enzyme shares 66% sequence identity with PTP1B and exhibits a reduced activity when its C-terminal helix is removed (Fig. 3a and Supplementary

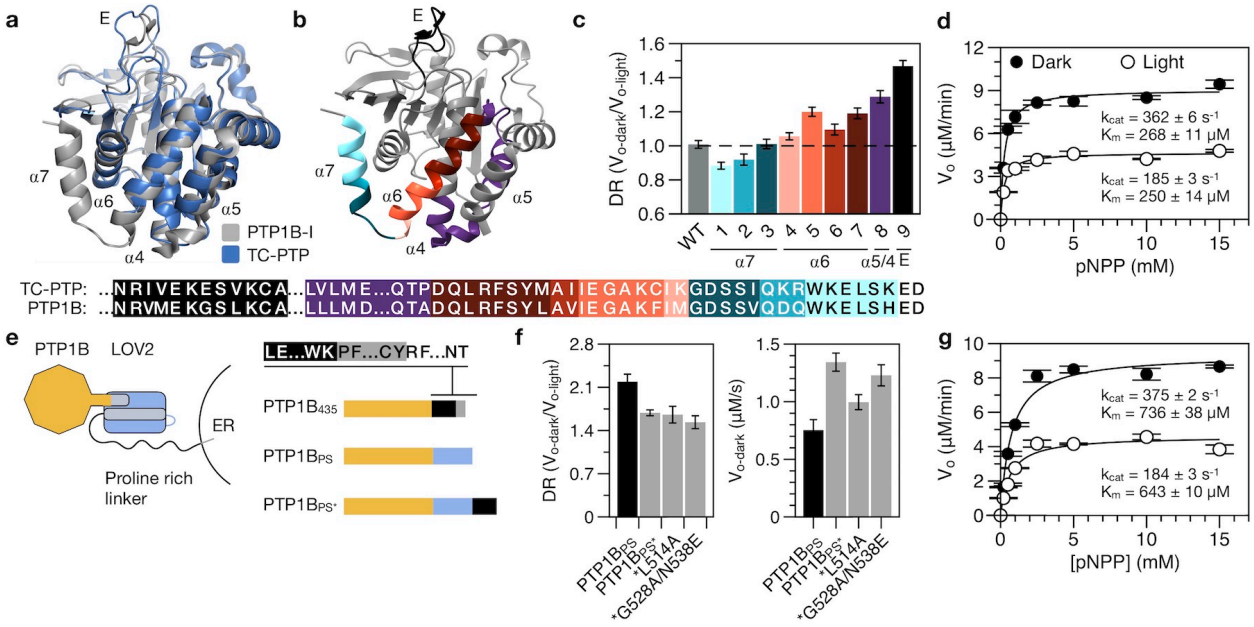

Figure 3 | Extension of photocontrol. **a**, Aligned structures of TCPTP (1l8k) and competitively inhibited PTP1B (PDB entry 2f71). **b**, Highlights show regions of PTP1B introduced sequentially into TCPTP-LOV2 chimeras: For example, chimera 1 includes only the light blue region of PTP1B; chimera 3 includes all blue regions. **c**, Kinetic measurements of chimeras on 4MUP. The DR increases as chimeras become more "PTP1B-like" (i.e., 1 to 9). **d**, Saturation curves show the activity of construct 9 on pNPP ($k_{cat\text{-}dark}/k_{cat\text{-}light}$ = 1.96 +/- 0.05). **e**, We attached the C-terminal residues of full-length PTP1B (i.e., residues 299-405, which include a disordered proline-rich region, but do not the ER anchor) to the C-terminus of $PTP1B_{PS}$. **f**, The final construct, termed $PTP1B_{PS}^{*}$, is photoswitchable but exhibits a reduced DR; mutations that stabilize the Jα helix do not improve DR. **g,** Saturation curves show the activity of $PTP1B_{PS*}$ on pNPP ($k_{cat\text{-}dark}/k_{cat\text{-}light}$ = 2.03 +/- 0.04). Error bars in **c**, **d**, **f**, and **g** denote SE with n ≥ 6 independent reactions. Exact sample sizes appear in Supplementary Tables 3 and 4.

Fig. 3b). Our first TCPTP-LOV2 chimera failed to express in *E. coli*, however, so we pursued a more aggressive design strategy: We searched for modulatory residues that might be unique to PTP1B by systematically modifying TCPTP to be more "PTP1B-like", starting from the C-terminus (Fig. 3b). Surprisingly, the sequential introduction of homologous segments of PTP1B led to a systematic increase in DR (Fig. 3c). The final chimera, which contained 25 residues from the α4-α7 helices and E loop of PTP1B, exhibited a DR of 2.03 on pNPP (Fig. 3d). This chimera, which leaves TCPTP 91.6% intact, may not be ideal for studying TCPTP-mediated signaling networks; the series of constructs used to develop it, however, reveals important differences in the allosteric networks of PTP1B and TCPTP. Our findings indicate that residues in the α4-α7 helices and E loop of PTP1B are necessary for α7-based control of its catalytic activity—a relationship supported by a recent NMR study, which showed that motions in the α4-α6 helices of PTP1B affect hydrolysis rate and product release[34]. Our results further suggest that the modulatory function of the α7 helix and/or the energetics of its conformational change, which involves delocalized conformational rearrangements[24], are not conserved across the PTP family. Broadly, our analysis demonstrates a novel approach for using optogenetic actuators as structural probes for studying—and comparing—allosteric control systems.

Preparation of a Natively Localized Variant of PTP1B$_{PS}$. Inside the cell, PTP1B possesses a C-terminal region—a disordered proline-rich domain followed by a short membrane anchor—that localizes it to the endoplasmic reticulum (ER; Fig. 3e)[35]. To examine the influence of this region on photocontrol, we attached the bulk of it (all but the hydrophobic ER anchor) to the C-terminus of PTP1B$_{PS}$ and assayed the extended chimera *in vitro*. This construct, termed PTP1B$_{PS*}$, exhibited a reduced DR, which was not improved by the addition of stabilizing

mutations to the Jα helix (Figs. 3f-3g); to our satisfaction, however, the addition of the full-length C-terminus (everything including the ER anchor) conferred native localization in COS-7 cells (Supplementary Fig. 4).

We completed our characterization of the full-length construct by examining the influence of LOV2 on interactions mediated by its disordered C-terminal region. Briefly, we compared the susceptibilities of $PTP1B_{1\text{-}405}$ and $PTP1B_{PS*}$ to inhibition by DPM-1001, an inhibitor that binds preferentially to this region (Supplementary Fig. 4)[36]. To our surprise, IC_{50}'s differed by ~30%, a difference that indicates that LOV2 does not prevent regulatory interactions involving its disordered region. Intriguingly, DPM-1001 also binds weakly to the catalytic domain, likely by associating with the α7 helix[37]; IC_{50}'s for $PTP1B_{1\text{-}321}$ and $PTP1B_{PS}$ were, thus, much higher than IC_{50}'s for the full-length constructs and exhibited a greater sensitivity to LOV2. This light-sensitive domain may thus, affect weak regulatory interactions that occur at its exact point of attachment (although, such interactions have yet to be established).

An Optogenetic Probe for Studying Intracellular Signaling. To examine the function of PTP1B-LOV2 chimeras in living cells, we sought a genetically encodable sensor for PTP1B activity. Several previously developed sensors for PTKs could plausibly support such a function; we chose a sensor for Src kinase[38], an enzyme with an orthogonal activity to PTP1B[39]. This biosensor consists of an SH2 domain, a flexible linker, and a substrate domain (i.e., WMEDYDYVHLQG, a peptide derived from p130cas), all sandwiched between two fluorescent proteins (FPs). Src-mediated phosphorylation of the substrate domain causes it to bind to the SH2 domain, reducing Förster resonance energy transfer between the FPs (FRET; Fig. 4a);

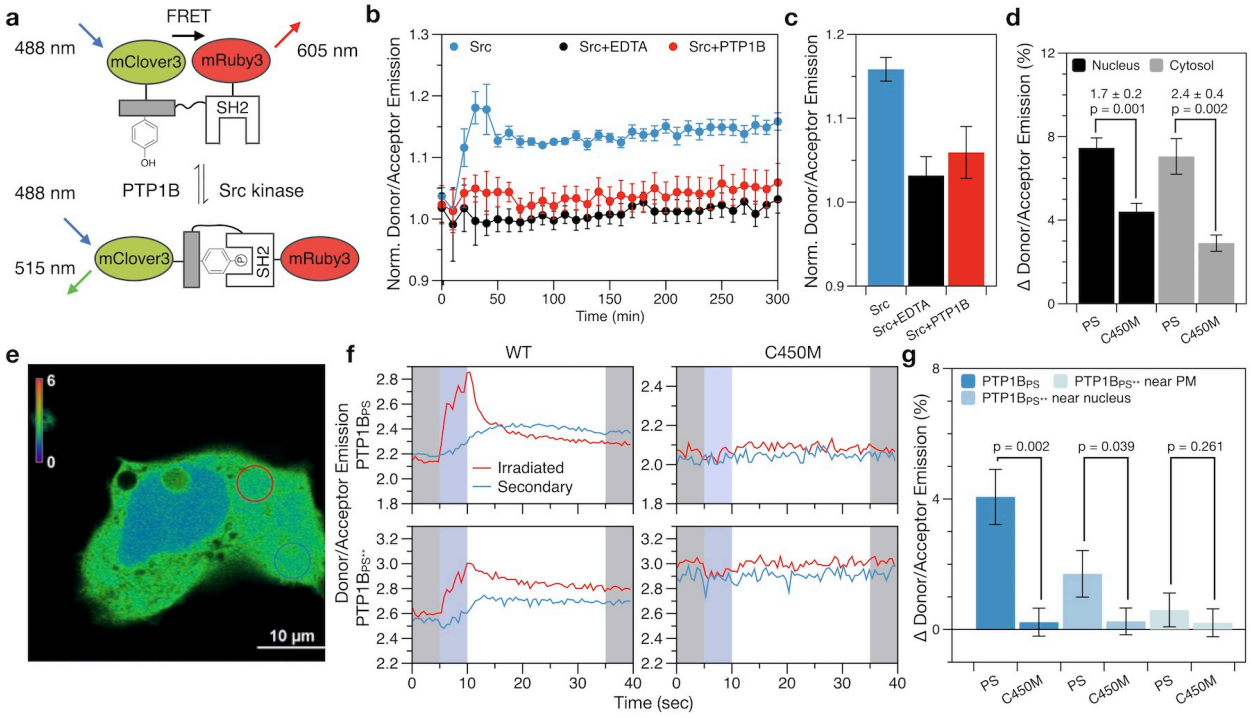

Figure 4 | Localized deactivation of PTP1B$_{PS}$. a, A biosensor for PTP1B activity. Src-mediated phosphorylation of the substrate domain causes it to bind SH2, triggering a conformational change that decreases FRET; dephosphorylation by PTP1B increases FRET. **b,** Src increases the donor/acceptor emission ratio *in vitro* (normalized by the buffer-only condition); EDTA or PTP1B prevent this increase. **c,** The signal from **b** at 300 min. **d,** The percent change in donor/acceptor emission ratio over 1 min within 5-μm circular regions located in the cytosol and nucleus of COS-7 cells activated with 457 nm light. Plots show the interquartile average and SE for n = 11 experiments. **e**, An image of localized illumination (405 nm) of a COS-7 cell expressing both PTP1B$_{PS}$ and biosensor. Circles delineate irradiated (red) and a secondary (blue) regions. **f**, Time courses of FRET in irradiated and secondary regions. Shading highlights 5-s periods before (gray), during (blue), and after (gray) illumination. **g**, The change in FRET between 5-s intervals measured before and after illumination (gray regions in **f**). For PTP1B$_{PS}$**, illumination near the nucleus, but not the plasma membrane (PM) causes a detectable change in

FRET. Error bars in **b**, **c**, **d**, and **g** denote SE for $n \geq 3$ (**b-d**) and $n = 6$ (**g**) independent experiments. Exact sample sizes for **b-d** appear in Supplementary Tables 8 and 9.

PTP1B-mediated dephosphorylation of the substrate domain, in turn, has the reverse effect and increases FRET. To enhance the compatibility of the sensor with the blue light necessary to stimulate LOV2, we replaced CFP and YPet—the original FPs—with mClover3 and mRuby3, which have longer excitation wavelengths[40]. As expected, incubation of the modified sensor with Src reduced FRET and increased the donor/acceptor emission ratio; simultaneous incubation with Src and PTP1B (or Src and EDTA), by contrast, prevented this response (Figs. 4b-4c).

We began our imaging studies by co-expressing the biosensor with PTP1B-LOV2 chimeras in COS-7 cells. These cells are large and flat and, thus, facilitate imaging of subcellular regions[41]; previous studies have used them to examine PTP1B-mediated signaling events[42,43]. Whole-cell irradiation of cells expressing $PTP1B_{PS}$ with 457 nm light increased the biosensor signal in both the nucleus and cytosol by ~7%, a change larger than the 3-4% increase afforded by the dark-state mutant (Fig. 4d and Supplementary Fig. 5); the response of the biosensor in cells expressing $PTP1B_{PS**}$, by contrast, was nearly imperceptible when compared to the dark-state analogue (Supplementary Fig. 6). We note: Our imaging experiments rely on basal Src activity (i.e., we do not overexpress this enzyme). Accordingly, our findings indicate that transient inactivation of PTP1B allows background concentrations of Src to effect a rapid increase in the population of phosphorylated biosensor (other kinases could certainly contribute to this response, but our chosen biosensor is fairly specific for Src[44]).

Local irradiation of photoswitchable enzymes can permit detailed studies of spatially dependent signaling events and, by minimizing cellular exposure to optical stimuli, reduce the background signal caused by photobleaching[10]. To assess the compatibility of our light-sensitive chimeras with spatiotemporal studies, we used 405-nm light to irradiate 5-µm circular regions within COS-7 cells, and we measured the response of the biosensor (Fig. 4e). In cells expressing

PTP1B$_{PS}$, local irradiation of the cytosol produced a transient spike in donor/acceptor emission ratio within the irradiated region and a modest, smooth increase in signal within a secondary region located far from the first (Fig. 4f and Supplementary Fig. 7); both irradiated and secondary regions maintained a similar increase in signal for at least 30 seconds after irradiation. In cells expressing PTP1B$_{PS**}$, irradiation near the nucleus produced a similar change in signal, while irradiation near the plasma membrane (PM) failed to do so (Fig. 4f and Supplementary Figs. 8 and 9). In all cases, dark-state mutants produced no detectable effect. Our results thus indicate that localized inactivation of PTP1B$_{PS}$ and nucleus-proximal PTP1B$_{PS**}$ can produce a measurable cell-wide increase in the phosphorylation state of their targets.

The ER is a vesicular network that extends unevenly from the nucleus of the cell. To determine if the reduced activity of PTP1B$_{PS**}$ near the PM results from the low abundance of ER in this region, we used BFP-Sec61β, a genetically encoded ER label[45], to measure the subcellular distribution of ER. As expected, the fluorescence of 5-μm circular regions located near the PM was 2.7-fold lower than the fluorescence of equivalently sized regions located near the nucleus (Supplementary Fig. 10); this discrepancy suggests that the diffuse distribution of PTP1B$_{PS**}$ near the PM limits the activity of this chimera on membrane-proximal targets.

DISCUSSION

The study of PTPs has long suffered from a paucity of tools for probing and measuring their intracellular activities[46]. In this study, we developed a photoswitchable variant of PTP1B and used it to exert spatiotemporal control over the phosphorylation state of a genetically encoded biosensor in living cells. Transient irradiation of the full-length, natively localized construct near the nucleus but not the PM produced cell-wide changes in sensor phosphorylation.

Most importantly, the changes in activity afforded by our allosteric control system reach—by our best estimate—70-85% of the maximum achievable dynamic range, and they match physiologically influential changes in activity caused by post-translational modifications of PTP1B that occur outside of the active site. Notably, insulin-stimulated sumoylation of its C-terminal disordered region reduces its activity by ~ 2.3-fold and disrupts its inhibition of both insulin receptor signaling and v-crk transformation[47]; our photoswitchable PTP1B provides a valuable tool for determining if this type of effect results entirely from a small reduction in enzyme activity (i.e., a reduction that we can recapitulate) or from other post-translationally derived influences (e.g., attenuation of protein-protein binding). Broadly, PTP1B is a therapeutic target for the treatment of diabetes, obesity, breast cancer[37] and has emerged as a potential modulator of inflammation[48], anxiety[49], immunity[50], and neural specification in embryonic stem cells[51]; by helping to resolve the contribution of PTP1B to these complex processes, the tools developed in this study could help to elucidate the biochemical basis—and, perhaps, shared origin—of a diverse set of physiological states.

Classical—or tyrosine-specific—PTPs possess several features that are particularly incompatible with other, more conventional approaches to optical control: Their solvent-exposed active sites are distal to both termini and, thus, difficult to obstruct with light-sensitive fusion partners [52]; they engage in protein-protein interactions at delocalized—and incompletely mapped—surface sites that make the physiological repercussions of domain insertion (or domain dissection) difficult to assess[53–55]; and their subcellular localization affects regulatory function in a non-binary manner that complicates the use of optically induced re-localization to study cell signaling[42,56]. Future efforts to use disruptive architectures to build photoswitchable PTPs with dynamic ranges that exceed those afforded by the constructs developed in this study could be

worthwhile, but they will benefit from analyses that show the effects of such architectures on protein structure, substrate specificity, binding affinity, and/or subcellular localization.

The results of this work offer two general insights for the design of genetically encoded probes. First, kinetic assays of $PTP1B_{PS}$ indicate that allosteric systems for photocontrol can enable isolated changes in k_{cat}; such designs are more likely to be substrate agnostic than systems in which light-sensitive domains act as competitive inhibitors (which can be outcompeted by a sufficiently high concentrations of substrate). Future analyses of differences in the intracellular concentrations and binding affinities of regulatory targets will clarify the extent of this benefit. Second, spectroscopic analyses of PTP1B-LOV2 chimeras provide experimental evidence that strong interdomain conformational coupling is necessary for allosterically-derived photocontrol. Computational methods to optimize this coupling (e.g., methods that enhance correlated motions between fused domains or that reduce the dissipation of energy between them) could facilitate the development of new varieties of photoswitchable enzymes.

Finally—and, perhaps, most intriguingly—this study demonstrates a new application for using optogenetic actuators in detailed biophysical studies. By analyzing photocontrol in systematically varied PTP-LOV2 chimeras, we identified residues necessary for α7-based control of catalytic activity. The pronounced influence of the E loop was particularly interesting, given the distance between this loop and the α7 helix. Our comparison of PTP1B and TCPTP thus indicates that efforts to extend allosteric photocontrol systems across protein families can reveal important differences in the allosteric networks of family members and suggests, broadly, that optogenetic actuators may provide an important source of structural probes—a kind of physical disruptive "ratchet"—for dissecting allosteric regulation within proteins.

METHODS

Methods, including statements of data availability and any associated accession codes, are available in the online version of this paper.

ACKNOWLEDGEMENTS

This work was supported by funds provided by the National Science Foundation (A.H. and J.M.F, CBET 1804897). The ALS-ENABLE beamlines, which were used for X-ray crystallography, are supported by the National Institutes of Health (award P30 GM124169-01). The Nikon A1R microscope used for laser scanning confocal microscopy is supported by the NIST-CU Cooperative Agreement (Award 70NANB15H226). The Advanced Light Source is a user facility sponsored by the Department of Energy's Office of Science (contract DE-AC02-05CH11231), and the Advanced Light Microscopy Core is a core facility supported by the BioFrontiers Institute. We thank Joe Dragavon for guidance on imaging studies and Annette Erbse for assistance with CD spectroscopy.

AUTHOR CONTRIBUTIONS

J.M.F. conceived of research. A.H. and J.M.F designed experiments. A.H. carried out cloning, protein expression, kinetic measurements, crystal growth, spectroscopic analyses, and imaging experiments. B.S. collected X-ray diffraction data. B.S. and P.Z. provided guidance on structural refinement. A.H. and J.M.F analyzed all data. A.H. and J.M.F. wrote the paper.

COMPETING INTERESTS

A.H. and J.M.F. are inventors on a PCT application that includes data from this manuscript.

ADDITIONAL INFORMATION

Supplementary information is available in the online version of this paper.

ONLINE METHODS

Cloning and molecular biology. We constructed PTP1B-LOV2 chimeras by fusing PTP1B and LOV2 at homologous crossover points. In brief, we used EMBOSS Needle, an implementation of the Needleman-Wunsch algorithm[57], to align the C-terminus of PTP1B (residues 285-305) with the N-terminus of LOV2 (residues 387-410), and we selected eight matching aligned residues as fusion points for the two domains (Fig. 1b). To assemble chimeric genes, we amplified DNA encoding PTP1B and LOV2 from pET21b and pTriEx-PA-Rac1 plasmids, respectively. (The pET21b plasmid was a kind gift from the Tonks Group of Cold Spring Harbor Laboratory; we purchased pTriEx-PA-Rac1 from Addgene, Inc.). We joined the two amplified segments with overlap extension PCR (oePCR; see Supplementary Table 11 for primers) and ligated the final chimeric product into pET16b for protein expression.

We generated additional constructs with standard techniques. To build single-site mutants and truncation variants, we amplified parent plasmids with appropriate mutagenic primers (Supplementary Table 12). To assemble variants of TCPTP-LOV2, we aligned the N-terminus of $PTP1B_{PS}$ (residues 1-298) with TCPTP (residues 1-296), selected identical residues as fusion points (Fig. 3a), and used oePCR or Gibson assembly (50°C for 1 hr) to build chimeras (see Supplementary Table 13 for primers and Supplementary Table 15 for DNA fragments). To

construct PTP1B$_{PS*}$ and PTP1B$_{PS**}$, we amplified C-terminal regions of PTP1B (residues 299-405 and 299-435, respectively) from pGEX-2T-PTP1B (Addgene, Inc.) and used Gibson assembly to join them to the C-terminus of PTP1B$_{PS}$ (50°C for 1 hr; see Supplementary Table 15 for primers). Finally, to construct GFP-tagged versions of PTP1B$_{PS}$, PTP1B$_{PS**}$, and PTP1B$_{435}$, we amplified these genes from their parent plasmids (see Supplementary Table 14 for primers) and ligated the PCR product into pAcGFP1-C1 (Clonetech, Inc.) at the NcoI and BamHI sites of the MCS for protein expression.

We developed a LOV2-compatible biosensor for PTP1B by replacing the fluorescent proteins of a biosensor for Src kinase[38] with mClover3 and mRuby3[40]. In brief, we amplified (i) the DNA segment encoding the SH2 domain, interdomain linker, and substrate domain (i.e., WMEDYDYVHLQG, a peptide derived from p130cas) of the original biosensor (Kras-Src FRET biosensor, Addgene), (ii) the genes for mClover3 and mRuby3 (plasmids pNCS-mClover3 and pNCS-mRuby3, respectively), and (iii) the backbone of pAcGFP1-C1 (Clonetech, Inc.; see Supplementary Table 14 for primers), and we joined the final PCR products with Gibson assembly (50°C for 1 hr).

For live-cell studies, we integrated the modified biosensor and PTP1B-LOV2 chimeras into pAcGFP1-C1 by using protocols described above. In short, we used primers from Supplemental Tables 14 and 15 to amplify DNA encoding (i) PTP1B$_{PS}$ or PTP1B$_{PS**}$, (ii) a ribosomal skipping peptide sequence (P2A-GSG, GSGATNFSLLKQAGDVEENPGP), (iii) the modified biosensor, and (iv) the pAcGFP1-C1 backbone, and we joined the segments with Gibson assembly (50°C for 1 hr).

Protein expression and purification. We overexpressed $PTP1B_{1-281}$, $PTP1B_{1-321}$, $PTP1B_{1-405}$, $TCPTP_{1-281}$, $TCPTP_{1-317}$, $LOV2_{404-547-}$, PTP-LOV2 chimeras, $Src_{251-536}$, and the modified biosensor in *E. coli* by carrying out the following steps: (i) We subcloned 6x polyhistidine-tagged versions of each construct into a pET16b plasmid. For both Src and the biosensor, we used an N-terminal tag; for everything else, we used a C-terminal tag. For Src, we also added a gene for Cdc37, a chaperone that facilitates protein folding in bacteria[58]. (ii) We transformed BL21(DE3) *E. coli* cells with each plasmid and spread the transformed cells onto an agar plate (25 g/L LB, 100 mg/L carbenicillin, 1.5% agar). (iii) We used one colony from each plate to inoculate a 20-mL culture (25 g/L LB and 100 mg/L carbenicillin), which we incubated in a shaker at 37°C overnight. (iv) We used the overnight culture to inoculate 1 L of induction media (20 g/L tryptone, 10 g/L yeast extract, 5 g/L NaCl, 4 g/L M9 slats, 4 g/L glucose, and 100 mg/L carbenicillin), which we incubated in a shaker at 37°C until it reached an OD_{600} of ~0.6. (v) We induced protein expression by adding 100 µL of 1 M solution of isopropyl β-D-1-thiogalactopyranoside (IPTG) to each culture and by reducing the temperature to 22°C. (vi) At 7 h, we pelleted cells (4,000 rpm, 20 min).

We purified all proteins with fast protein liquid chromatography. To begin, we lysed cell pellets by adding the following components to each gram of pellet: 4 mL of B-PER (Thermo Fisher Scientific, Inc.), 1 mg $MgSO_4$, 2 mg Nα-p-Tosyl-L-arginine methyl ester hydrochloride, 1.25 mg tris(2-carboxyethyl)phosphine (TCEP), 3.75 µl phenylmethylsulfonyl fluoride, 1 mg Lysozyme, and 10 µl DNase. After mixing to homogeneity, we rocked the lysis mixtures for 1 h at room temperature (~22°C), pelleted the cell debris (6,000 rpm, 60 min), and isolated the supernatant. To clarify the supernatant further, we added a saturated solution of ammonium sulfate to 10% (v/v), pelleted the resulting mixture (6,000 rpm, 15 min), and used a 0.22-µm

filter to remove particulates. To begin purification, we exchanged the filtered supernatant into Tris-HCl buffer (50 mM Tris-HCl, 0.5 mM TCEP, pH 7.5), flowed the exchanged solution over an Ni column, and eluted the protein of interest with a 0-100% gradient of imidazole (50 mM Tris-HCl, 0.5 mM TCEP, 500 mM imidazole, pH 7.5). For further purification, we exchanged each protein into HEPES buffer (50 mM HEPES, 0.5 mM TCEP, pH 7.5), flowed the exchanged solution over an anion exchange column, and eluted the final protein with 0-100% gradient of NaCl (50 mM HEPES, 0.5 mM TCEP, 500 mM NaCl, pH 7.5). We purchased all columns [26/10 HiPrep (desalting), HisTrap HP (Ni), and HiPrep Q HP 16/10 (anion exchange)] from GE Healthcare, Inc. We confirmed the purity of final solutions with SDS-PAGE, and we stored each protein in storage buffer (50 mM HEPES, 0.5 mM TCEP, 20 v/v% glycerol, pH 7.5) at -80°C.

Initial analysis of photoswitching. We screened PTP-LOV2 chimeras for light-dependent catalytic activity by measuring their activity on 4MUP in the presence and absence of light. In brief, we carried out the following steps: (i) In a room illuminated with a red light (625 nm), we prepared two 96-well plates—hereafter referred to as the "light plate" and "dark plate"—with 100-µL reactions consisting of buffer (50 mM HEPES, 0.5 mM TCEP, pH 7.5), substrate (500 µM 4MUP), and enzyme (5 nM); we added a plastic cover to each plate. (ii) We encased the dark plate in foil and placed the light plate in a chamber made up of two opposing reflective steel bowls fed with a 455-nm light (~450 mW, SLS-0301-C, Mightex Systems, Inc.; Supplementary Fig. 1d-1f). (iii) We incubated both plates at room temperature (~22°C). (iv) At 7, 14, 21, 28, 35 and 42 minutes after beginning the reaction, we removed each plate from its resting position (i.e., the foil cover or light chamber), loaded it into a SpectraMax M2 plate reader, and measured the formation of 4-methylumbelliferone ($365_{ex}/450_{em}$); we immediately returned each plate to its

resting position. (v) We used discrete measurements to estimate initial rates and, thus, to calculate DR (i.e., $V_{o\text{-}dark}/V_{o\text{-}light}$; Supplementary Table 4). Error in our final estimates of DR reflects standard error (SE) propagated from plate-specific measurements of initial rates (Supplementary Table 4).

We minimized error in our measurements of photoswitching with four precautions: (i) We used concentrations of enzyme and substrate that sustained initial reaction rates for 42 minutes, a length of time that minimizes the disruption of 1-min breaks required to measure product formation. (ii) For each construct in each plate, we prepared six compositionally identical, yet differentially positioned wells; this arrangement minimizes potential contributions from nonuniform illumination. (iii) For each construct at each illumination condition, we repeated the assay at least three times, collecting a total of 18 measurements of initial rate (e.g., we collected 18 measurements of the activity of $PTP1B_{PS}$ on 4MUP in the light). (iv) We established a control range: When wild-type PTP1B, which was present in each plate, exhibited a 10% difference in activity between the two plates, we discarded data from both (i.e., we assumed that differences in activity between the two plates were not caused by the presence or absence of light).

We examined the light-dependent catalytic activity of $PTP1B_{PS}$ on a phosphopeptide (DADEpYLIPQQG from EGFR) by following the aforementioned procedure with several differences: (i) We used a substrate concentration of 120 μM and a total reaction volume of 40 uL. (ii) We added malachite green solution (Sigma-Aldrich) to stop individual reactions at 2, 4, 6, or 8 minutes. (iii) We measured the formation of phosphate by using the plate reader to quantify a complex formed between orthophosphate, molybdate, and Malachite Green (620_{abs}); we waited until the end of our experiments (i.e., 8 minutes) for all absorbance measurements.

Errors in final estimates of DR reflect SE propagated from plate-specific measurements of initial rates. We note: the statistically indistinguishable DRs ($p < 0.01$) determined for $PTP1B_{PS}$ on substrates that require different spectrophotometric measurements (i.e., fluorescence at 450 nm for 4MUP and absorbance at 620 nm for a phosphopeptide) suggest that the optical measurement methods do not, themselves, artificially depress or enhance DR.

Enzyme kinetics. We examined the influence of photomodulation on enzyme kinetics by measuring the activities of $PTP1B_{PS}$, $PTP1B_{PS*}$, and TCPTP-LOV2 (chimera 9) on pNPP in the presence and absence of light (i.e., we used dark and light plates as described above). Briefly, we prepared 100-µL reactions consisting of buffer (50 mM HEPES, 0.5 mM TCEP, pH 7.5), substrate (0.2, 0.5, 1, 2.5, 5, 10 and 15 mM pNPP), and enzyme (25 nM); at 4, 8, 12, 16 and 20 minutes after initiating the reaction, we measured the production of p-nitrophenol (405_{abs}) on a SpectraMax M2 plate reader; and we used DataGraph to fit initial rates to a Michaelis-Menten model of enzyme kinetics. Final values of k_{cat} and K_M reflect the mean of independent estimates determined from three Michaelis-Menten curves; error k_{cat} and K_M reflects the standard error of those estimates.

We examined the inhibitory effect of DPM-1001 on $PTP1B_{1-405}$, $PTP1B_{PS*}$, $PTP1B_{321}$, and $PTP1B_{PS}$ on pNPP as follows: (i) We carried out the aforementioned pNPP reactions in the presence of different concentrations of DPM-1001 (0, 20, 40, 60 µM for $PTP1B_{1-405}$ and $PTP1B_{PS*}$; 0, 100, 200, 400 µM for $PTP1B_{321}$ and $PTP1B_{PS}$). (ii) We used MATLAB's "nlinfit" and "fminsearch" functions to fit (a) initial-rate measurements collected in the absence of inhibitors to a Michaelis−Menten model and (b) initial-rate measurements collected in the presence and absence of inhibitors to four models of inhibition (i.e., competitive,

noncompetitive, uncompetitive, and mixed as described previously[59]). (iii) We used an F- test to compare the fits of (a) a mixed model, which has two parameters, and (b) each nested single-parameter model with the lowest sum of squared errors for a given dataset. DPM-1001 exhibited mixed inhibition for all constructs ($p < 0.01$). (iv) We estimated IC_{50}'s by using the best-fit kinetic model to determine the inhibitor concentration required to reduce initial rates by 50% on 15 mM pNPP. This high substrate concentration minimizes the concentration dependence of IC_{50}'s. We used the MATLAB function "nlparci" to determine the confidence intervals of kinetic parameters and propagated those intervals to estimate the corresponding confidence on IC_{50}'s.

We compared the activities of $PTP1B_{1-281}$, $PTP1B_{1-321}$, $TCPTP_{1-281}$, and $TCPTP_{1-317}$ on pNPP by using a continuous assay. Briefly, we prepared 100-µL reactions consisting of buffer (50 mM HEPES, 0.5 mM TCEP, pH 7.5), pNPP (0.2, 0.5, 1, 2.5, 5, 10 and 15 mM), and enzyme (25 nM); we measured the production of p-nitrophenol at five-second intervals for 270 seconds (SpectraMax M2 plate reader); and we used DataGraph to fit initial rates to a Michaelis-Menten model. Final values of k_{cat} and K_M reflect the mean of independent estimates determined from three Michaelis-Menten curves; error k_{cat} and K_M reflects the standard error of those estimates.

Finally, we evaluated the reversibility of our LOV2-based light switch by illuminating 25 uM of $PTP1B_{PS}$ (50 mM HEPES, 0.5 mM TCEP, pH 7.5) for 10 seconds and by, subsequently, monitoring its activity on 5 mM pNPP after 5 minutes in the dark. To minimize error, we repeated this experiment three times with seven cycles per experiment (Supplementary Fig. 2). Exact sample sizes for all kinetic data are reported in Supplementary Table 4.

X-ray crystallography. We prepared crystals of $PTP1B_{PS}$ by using hanging drop vapor diffusion. To begin, we prepared a concentrated solution of $PTP1B_{PS}$ (~400 µM $PTP1B_{PS}$, 50

mM HEPES, pH 7.3) and a crystallization solution (100 mM HEPES, 200 mM magnesium acetate, and 14% polyethylene glycol 8000, pH 7.5); we mixed the two solutions in 1:2, 1:3, and 1:6 ratios (protein: crystallization) to form 7-9 µl droplets for crystal growth; and we incubated the droplets over reservoirs filled with crystallization solution at 4℃ in the dark. Long hexagonal crystals with a yellow hue appeared after 1-3 weeks. Prior to freezing, we soaked all crystals in cryoprotectant (100 mM HEPES, 200 mM magnesium acetate, and 25% polyethylene glycol 8000, pH 7.5) overnight.

We collected X-ray diffraction through the Collaborative Crystallography Program of the Berkeley Center for Structural Biology, and we solved crystal structures as described previously[60]. Briefly, we performed integration, scaling, and merging of XRD data with the xia2 software package, and we carried out molecular replacement with the Phenix graphical user interface, followed by one round of PDB-REDO[61]. The crystallographic data collected in this study are reported in Supplementary Table 3.

Circular dichroism spectroscopy. We examined the influence of photomodulation on the secondary structure of PTP1B-LOV2 chimeras by using a circular dichroism spectrophotometer (Applied Photophysics Chirascan Plus) to measure optically induced changes in α-helical content. To collect full-spectrum measurements, we incubated 0.2 g/L solutions of each chimera (10 mM NaPi, 0.5 mM TCEP, pH 7.5) in a crystal cuvette (0.05-cm path length) for 10 seconds with/without blue light (455 nm) and immediately measured mean residue ellipticity (MRE) at 1-nm increments from 185 to 260 nm. To measure thermal recovery, we began as before, but we measured MRE at 222 nm every 2.5 seconds for 250 seconds in the dark. We normalized the CD data thus gathered with Eq. 1, where CD_t, CD_0, CD_{250} represent MRE at t, 0, and 250

$$\Delta CD_n = \frac{CD_t - CD_0}{CD_{250} - CD_0} \quad \text{(Eq. 1)}$$

$$\Delta CD_n = e^{-kt} \quad \text{(Eq. 2)}$$

seconds; and we fit the normalized data to an equation for exponential decay (Eq. 2). Final values of k reflect the mean and standard error of values determined from fits to six data sets (Supplementary Table 7).

Fluorescence spectroscopy. To examine the influence of photomodulation on the conformation of PTP1B within PTP1B-LOV2 chimeras, we use fluorescence spectroscopy to measure optically induced changes in tryptophan fluorescence. In brief, we prepared 60 μM solutions of protein (50 mM HEPES, 0.5 mM TCEP, pH 7.5) in a Helma ultra-micro quartz cuvette (Thomas Scientific, Inc.); we illuminated those solutions for 10 seconds with a 455-nm light; and we monitored fluorescence ($280_{ex}/365_{em}$) in 10-second intervals for 200 seconds using a SpectraMax M2 plate reader. We normalized the fluorescence data, thus gathered, with Eq. 3, where W_t, W_0,

$$W_n = \frac{W_t - W_0}{W_{250} - W_0} \quad \text{(Eq. 3)}$$

$$W_n = e^{-kt} \quad \text{(Eq. 4)}$$

W_{250} represent the emission at *t*, 0, and 250 seconds; and we fit the normalized data to an equation for exponential decay (Eq. 4). Final values of k reflect the mean and standard error of values determined from fits to six datasets (Supplementary Table 8).

Biosensor development. We assessed the sensitivity of an Src biosensor[38] to the activity of PTP1B by incubating it with Src in the presence and absence of PTP1B. In brief, we prepared

100-µL reactions consisting of 2 µM biosensor and 300 nM Src kinase in 1X kinase buffer A (Thermo Fisher Scientific, Inc.) supplemented with 2 mM DTT, 2 mM $MgCl_2$, and 50 µM ATP. For a subset of reactions, we added PTP1B and EDTA at concentrations of 100 nM and 50 mM, respectively. For each reaction, we monitored the fluorescence of mClover3 ($475_{ex}/520_{em}$) and mRuby3 ($475_{ex}/600_{em}$ nm) in 10-min increments for 300 minutes on a Spectramax M2 plate reader.

Cell culture. For live-cell imaging experiments, we grew COS-7 cells (ATCC CRL-1651, seeded from a freezer stock) in DMEM media supplemented with 10% FBS and 1% penicillin/streptomycin for ~24 hr to achieve 70-90% confluency, and we seeded them on a 20-mm glass-bottom cell culture dish (MatTek). At 10-20 hours after seeding, we depleted endogenous PTP1B by transfecting the cells with 25 nM of a PTP1B siRNA silencer (AM16794, Thermo Fisher Scientific, Inc.), 12.5 µl Dharmafect, and 10% FBS as described previously[45]. At 5 hours after adding siRNA, we washed cells with 1X PBS buffer, replaced this buffer with DMEM media supplemented with 10% FBS and 1% penicillin/streptomycin, and transfected the cells with 2000 ng of plasmid DNA and 6 µl of Lipofectamine 2000 reagent (Invitrogen) according to the manufacturer's protocols. At 10-12 hour after transfection with plasmid DNA, we imaged the cells in Opti-MEM media at 37°C.

Confocal microscopy. We carried out all imaging experiments with a 100x 1.45 NA oil objective on a Nikon A1R confocal scanning microscope supplemented with an environmental chamber (37°C, 75% humidity, and 5% CO_2; Pathology Devices, Inc.). To localize both GFP-tagged PTP1B-LOV2 chimeras and BFP-Sec61β, we illuminated Cos-7 cells with a 488-nm laser

(0.57 mW/μm^2 with a pixel dwell time of 2.2 μs) and imaged them with a 525/50 nm bandpass filter. The plasmid bearing BFP-Sec61β (pTagBFP-C1) was a kind gift from the lab of Gia Voeltz of the University of Colorado, Boulder.

For whole-cell activation studies, we illuminated individual cells with a 457-nm laser focused over the breadth of the cell (0.14 mW/μm^2 with a pixel dwell time of 4.8 μs). To examine the photoresponse of the biosensor after activation, we illuminated the field of view with a 488 nm laser (0.57 mW/μm^2) and imaged the entire cell with 525/50 nm and 600/50 nm bandpass filters for 1 minute (resonant scanning mode with 518.1-ms frame time). We estimated the average change in donor/acceptor emission ratio between 0 and 60 seconds after activation by calculating the interquartile average of 11 independent measurements (i.e., 11 individual cells).

For localized activation studies, we focused 405-nm light over 5-μm circular regions (0.49 mW/μm^2 with a pixel dwell time of 4.8 μs) and imaged the photoresponse of the biosensor by illuminating at 488 nm (0.57 mW/μm^2; 480/30 nm excitation filter) and imaging with 525/50 nm and 600/50 nm bandpass filters for 1 minute. We estimated the average change in donor/acceptor emission ratio within circular regions, in turn, by calculating the difference in 5-second averages starting (i) 5 seconds before activation and (ii) 35 seconds after activation; final estimates of changes in donor/acceptor emission reflect the mean and standard error from six independent measurements (i.e., six individual cells).

The 488-nm light used to image our FRET-based biosensor could plausibly stimulate LOV2, which absorbs at 488 nm (although less so than at 405 and 457 nm)[62]. The results of Figure 4f, however, indicate that such activation does not occur. In brief, irradiation with 405-nm light causes a transient increase in FRET signal for cells expressing PTP1B$_{PS}$ and PTP1B$_{PS**}$, but

not for cells expressing light-insensitive analogues of these two constructs; accordingly, 488-nm light does not activate LOV2 (at least, no fully) under our imaging conditions (if it did so, irradiation at 405 nm would not elicit further activation). The insensitivity of LOV2 to 488-nm light likely results from both (i) the low extinction coefficient of LOV2 at 488 nm and (ii) the insufficient combination of power and pixel dwell time of the 488-nm laser.

Reporting summary. Additional information on experimental design is available in the Nature Research Reporting Summary.

Statistical analysis. We used an F-test to compare one- and two-parameter models of inhibition. For all other analyses, we determined statistical significance by using a two-tailed Student's t test.

Data availability. The crystal structure determined in this study can be downloaded from the RCSB Protein Data Bank (PDB entry 6ntp; http://www.rcsb.org/). Source data for our figures is available as follows: Supplementary Table 4 (Fig. 1c, 1f, 2a, 3c, and 3f), Supplementary Table 5 (Figs. 1e, 3d, and 3g), Supplementary Table 7 (Fig. 2c), Supplementary Table 8 (Fig. 2g), Supplementary Table 9 (Figs. 4b and 4c), Supplementary Table 10 (Fig. 4d), and Supplementary Figs 7-9 (Fig. 4g). All other raw data not included in the manuscript are available from the corresponding author upon request.

REFERENCES

1. Wray, J. *et al.* Inhibition of glycogen synthase kinase-3 alleviates Tcf3 repression of the pluripotency network and increases embryonic stem cell resistance to differentiation. *Nat. Cell Biol.* **13**, 838–45 (2011).
2. Angers-Loustau, A. *et al.* Protein tyrosine phosphatase-PEST regulates focal adhesion disassembly, migration, and cytokinesis in fibroblasts. *J. Cell Biol.* **144**, 1019–1031 (1999).
3. Liu, H. *et al.* PTP1B promotes cell proliferation and metastasis through activating src and ERK1/2 in non-small cell lung cancer. *Cancer Lett.* **359**, 218–225 (2015).
4. Danial, N. N. & Korsmeyer, S. J. Cell Death: Critical Control Points. *Cell* **116**, 205–219 (2004).
5. Lessard, L., Stuible, M. & Tremblay, M. L. The two faces of PTP1B in cancer. *Biochimica et Biophysica Acta - Proteins and Proteomics* **1804**, 613–619 (2010).
6. Stanford, S. M. *et al.* Diabetes reversal by inhibition of the low-molecular-weight tyrosine phosphatase. *Nat. Chem. Biol.* **13**, 624–632 (2017).
7. Heneka, M. T., Golenbock, D. T. & Latz, E. Innate immunity in Alzheimer's disease. *Nat. Immunol.* **16**, 229–236 (2015).
8. Volinsky, N. & Kholodenko, B. N. Complexity of receptor tyrosine kinase signal processing. *Cold Spring Harb. Perspect. Biol.* **5**, a009043 (2013).
9. Kennedy, M. B. Signal-Processing Machines at the Postsynaptic Density. *Science.* **290**, 750–754 (2000).

10. Repina, N. A., Rosenbloom, A., Mukherjee, A., Schaffer, D. V. & Kane, R. S. At Light Speed: Advances in Optogenetic Systems for Regulating Cell Signaling and Behavior. *Annu. Rev. Chem. Biomol. Eng.* **8**, 13–39 (2017).

11. Gautier, A. *et al.* How to control proteins with light in living systems. *Nat. Chem. Biol.* **10**, 533–41 (2014).

12. Wu, Y. I. *et al.* A genetically encoded photoactivatable Rac controls the motility of living cells. *Nature* **461**, 104–108 (2009).

13. Zhou, X. X., Fan, L. Z., Li, P., Shen, K. & Lin, M. Z. Optical control of cell signaling by single-chain photoswitchable kinases. *Science.* **355**, 836–842 (2017).

14. Dagliyan, O. *et al.* Engineering extrinsic disorder to control protein activity in living cells. *Science.* **354**, 1441–1444 (2016).

15. Wang, H. *et al.* LOVTRAP: An optogenetic system for photoinduced protein dissociation. *Nat. Methods* **13**, 755–758 (2016).

16. Taslimi, A. *et al.* Optimized second-generation CRY2-CIB dimerizers and photoactivatable Cre recombinase. *Nat. Chem. Biol.* **12**, 425–430 (2016).

17. Bourdeau, A., Dubé, N. & Tremblay, M. L. Cytoplasmic protein tyrosine phosphatases, regulation and function: The roles of PTP1B and TC-PTP. *Current Opinion in Cell Biology* **17**, 203–209 (2005).

18. Whittier, S. K., Hengge, A. C. & Loria, J. P. Conformational Motions Regulate Phosphoryl Transfer in Related Protein Tyrosine Phosphatases. *Science.*. **341**, 899–903 (2013).

19. Cortesio, C. L. *et al.* Calpain 2 and PTP1B function in a novel pathway with Src to regulate invadopodia dynamics and breast cancer cell invasion. *J. Cell Biol.* **180**, 957–971 (2008).

20. Liu, F. & Chernoff, J. Protein tyrosine phosphatase 1B interacts with and is tyrosine phosphorylated by the epidermal growth factor receptor. *Biochem. J.* **327**, 139–145 (2015).

21. Leopold, A. V., Chernov, K. G. & Verkhusha, V. V. Optogenetically controlled protein kinases for regulation of cellular signaling. *Chemical Society Reviews* (2018).

22. Chang, K. Y. *et al.* Light-inducible receptor tyrosine kinases that regulate neurotrophin signalling. *Nat. Commun.* (2014).

23. Halavaty, A. S. & Moffat, K. N- and C-terminal flanking regions modulate light-induced signal transduction in the LOV2 domain of the blue light sensor phototropin 1 from Avena sativa. *Biochemistry* **46**, 14001–14009 (2007).

24. Choy, M. S. *et al.* Conformational Rigidity and Protein Dynamics at Distinct Timescales Regulate PTP1B Activity and Allostery. *Mol. Cell* **65**, 644–658 (2017).

25. Levskaya, A. *et al.* Synthetic biology: engineering Escherichia coli to see light. *Nature* **438**, 441–2 (2005).

26. Strickland, D. *et al.* Rationally improving LOV domain-based photoswitches. *Nat. Methods* **7**, 623–6 (2010).

27. Cosentino, C. *et al.* Engineering of a light-gated potassium channel. *Science.* **348**, 707–710 (2015).

28. Pace, C. N. & Scholtz, J. M. A helix propensity scale based on experimental studies of peptides and proteins. *Biophys. J.* **75**, 422–427 (1998).

29. Buckley, A. M., Petersen, J., Roe, A. J., Douce, G. R. & Christie, J. M. LOV-based reporters for fluorescence imaging. *Curr. Opin. Chem. Biol.* **27**, 39–45 (2015).

30. Gehrig, S. *et al.* An engineered photoswitchable mammalian pyruvate kinase. *FEBS J.* **284**, 2955–2980 (2017).

31. Zayner, J. P., Antoniou, C. & Sosnick, T. R. The amino-terminal helix modulates light-activated conformational changes in AsLOV2. *J. Mol. Biol.* **419**, 61–74 (2012).

32. Harper, S. M., Christie, J. M. & Gardner, K. H. Disruption of the LOV-Jα helix interaction activates phototropin kinase activity. *Biochemistry* **43**, 16184–16192 (2004).

33. Hjortness, M. K. *et al.* Evolutionarily Conserved Allosteric Communication in Protein Tyrosine Phosphatases. *Biochemistry* **57**, 6443–6451 (2018).

34. Cui, D. S., Lipchock, J. M., Brookner, D. & Loria, J. P. Uncovering the Molecular Interactions in the Catalytic Loop That Modulate the Conformational Dynamics in Protein Tyrosine Phosphatase 1B. *J. Am. Chem. Soc.* (2019).

35. Frangioni, J. V., Beahm, P. H., Shifrin, V., Jost, C. A. & Neel, B. G. The nontransmembrane tyrosine phosphatase PTP-1B localizes to the endoplasmic reticulum via its 35 amino acid C-terminal sequence. *Cell* (1992).

36. Krishnan, N., Konidaris, K. F., Gasser, G. & Tonks, N. K. A potent, selective, and orally bioavailable inhibitor of the protein-tyrosine phosphatase PTP1B improves insulin and leptin signaling in animal models. *J. Biol. Chem.* **293**, 1517–1525 (2018).

37. Krishnan, N. *et al.* Targeting the disordered C terminus of PTP1B with an allosteric inhibitor. *Nat. Chem. Biol.* **10**, 558–566 (2014).

38. Ouyang, M., Sun, J., Chien, S. & Wang, Y. Determination of hierarchical relationship of Src and Rac at subcellular locations with FRET biosensors. *Proc Natl Acad Sci U S A* **105**, 14353–14358 (2008).

39. Montalibet, J. *et al.* Residues distant from the active site influence protein-tyrosine phosphatase 1B inhibitor binding. *J. Biol. Chem.* **281**, 5258–5266 (2006).

40. Bajar, B. T. *et al.* Improving brightness and photostability of green and red fluorescent proteins for live cell imaging and FRET reporting. *Sci. Rep.* **6**, 20889 (2016).

41. Fehr, M., Lalonde, S., Lager, I., Wolff, M. W. & Frommer, W. B. In vivo imaging of the dynamics of glucose uptake in the cytosol of COS-7 cells by fluorescent nanosensors. *J. Biol. Chem.* **278**, 19127–19133 (2003).

42. Yudushkin, I. A. *et al.* Live-cell imaging of enzyme-substrate interaction reveals spatial regulation of PTP1B. *Science* **315**, 115–119 (2007).

43. Zabolotny, J. M. *et al.* PTP1B regulates leptin signal transduction in vivo. *Dev. Cell* **2**, 489–495 (2002).

44. Wang, Y. *et al.* Visualizing the mechanical activation of Src. *Nature* **434**, 1040–1045 (2005).

45. Rowland, A. A., Chitwood, P. J., Phillips, M. J. & Voeltz, G. K. ER contact sites define the position and timing of endosome fission. *Cell* **159**, 1027–1041 (2014).

46. Yao, Z. *et al.* A Global Analysis of the Receptor Tyrosine Kinase-Protein Phosphatase Interactome. *Mol. Cell* **65**, 347–360 (2017).

47. Dadke, S. *et al.* Regulation of protein tyrosine phosphatase 1B by sumoylation. *Nat. Cell Biol.* **9**, 80–85 (2007).

48. Través, P. G. *et al.* Pivotal role of protein tyrosine phosphatase 1B (PTP1B) in the macrophage response to pro-inflammatory and anti-inflammatory challenge. *Cell Death Dis.* **5**, e1125 (2014).

49. Qin, Z. *et al.* Chronic Stress Induces Anxiety via an Amygdalar Intracellular Cascade that Impairs Endocannabinoid Signaling. *Neuron* **85**, 1319–1331 (2015).

50. Shuai, K. & Liu, B. Regulation of JAK-STAT signalling in the immune system. *Nat. Rev. Immunol.* **3**, 900–911 (2003).

51. Matulka, K. *et al.* PTP1B is an effector of activin signaling and regulates neural specification of embryonic stem cells. *Cell Stem Cell* **13**, 706–719 (2013).

52. Barr, A. J. *et al.* Large-Scale Structural Analysis of the Classical Human Protein Tyrosine Phosphatome. *Cell* **136**, 352–363 (2009).

53. Li, S., Depetris, R. S., Barford, D., Chernoff, J. & Hubbard, S. R. Crystal structure of a complex between protein tyrosine phosphatase 1B and the insulin receptor tyrosine kinase. *Structure* **13**, 1643–1651 (2005).

54. Pádua, R. A. P. *et al.* Mechanism of activating mutations and allosteric drug inhibition of the phosphatase SHP2. *Nat. Commun.* **9**, 4507 (2018).

55. Bakke, J. & Haj, F. G. Protein-tyrosine phosphatase 1B substrates and metabolic regulation. *Semin. Cell Dev. Biol.* **37**, 58–65 (2015).

56. Eden, E. R., White, I. J., Tsapara, A. & Futter, C. E. Membrane contacts between endosomes and ER provide sites for PTP1B-epidermal growth factor receptor interaction. *Nat. Cell Biol.* **12**, 267–72 (2010).

57. Rice, P., Longden, L. & Bleasby, A. EMBOSS: The European Molecular Biology Open Software Suite. *Trends Genet.* **16**, 276–277 (2000).

58. Piserchio, A., Cowburn, D. & Ghose, R. Expression and purification of Src-family kinases for solution NMR studies. *Methods Mol. Biol.* **831**, 111–131 (2012).

59. Hjortness, M. K. *et al.* Abietane-Type Diterpenoids Inhibit Protein Tyrosine Phosphatases by Stabilizing an Inactive Enzyme Conformation. *Biochemistry* **57**, 5886–5896 (2018).

60. Hjortness, M. K. *et al.* Evolutionarily Conserved Allosteric Communication in Protein Tyrosine Phosphatases. *Biochemistry* **57**, 6443–6451 (2018).

61. Friesner, R. a. *et al.* Glide: A New Approach for Rapid, Accurate Docking and Scoring. 1. Method and Assessment of Docking Accuracy. *J. Med. Chem.* **47**, 1739–1749 (2004).

62. Swartz, T. E. *et al.* The Photocycle of a Flavin-binding Domain of the Blue Light Photoreceptor Phototropin. *J. Biol. Chem.* **276**, 36493–36500 (2001).